



**Turbulence structure  
in a cloud-topped  
boundary layer**

J. Tonttila et al.

# Turbulent structure and scaling of the inertial subrange in a stratocumulus-topped boundary layer observed by a Doppler lidar

J. Tonttila<sup>1,3</sup>, E. J. O'Connor<sup>2,4</sup>, A. Hellsten<sup>2</sup>, A. Hirsikko<sup>2,5</sup>, C. O'Dowd<sup>6</sup>,  
H. Järvinen<sup>3</sup>, and P. Räisänen<sup>2</sup>

<sup>1</sup>Finnish Meteorological Institute, Atmospheric Research Centre of Eastern Finland, P.O. Box 1627, 70211 Kuopio, Finland

<sup>2</sup>Finnish Meteorological Institute, P.O. Box 503, 00101, Helsinki, Finland

<sup>3</sup>University of Helsinki, Department of Physics, P.O. Box 48, 00014, Helsinki, Finland

<sup>4</sup>University of Reading, Reading, UK

<sup>5</sup>Forschungszentrum Jülich GmbH, Institut für Energie-und Klimaforschung: Troposphäre (IEK-8), Jülich, Germany

<sup>6</sup>School of Physics and Centre for Climate & Air Pollution Studies, Ryan Institute, National University of Ireland Galway, University Road, Galway, Ireland

Title Page

Abstract

Introduction

Conclusions

References

Tables

Figures



Back

Close

Full Screen / Esc

Printer-friendly Version

Interactive Discussion



Received: 29 August 2014 – Accepted: 5 September 2014 – Published: 18 September 2014

Correspondence to: J. Tonttila (juha.tonttila@fmi.fi)

Published by Copernicus Publications on behalf of the European Geosciences Union.

**ACPD**

14, 24119–24148, 2014

---

**Turbulence structure  
in a cloud-topped  
boundary layer**

J. Tonttila et al.

---

Title Page

Abstract

Introduction

Conclusions

References

Tables

Figures



Back

Close

Full Screen / Esc

Printer-friendly Version

Interactive Discussion



## Abstract

The turbulent structure of a stratocumulus-topped marine boundary layer over a two-day period is observed with a Doppler lidar at Mace Head in Ireland. Using profiles of vertical velocity statistics, the bulk of the mixing is identified as cloud-driven. This is supported by the pertinent feature of negative vertical velocity skewness in the sub-cloud layer which extends, on occasion, almost to the surface. Both coupled and decoupled turbulence characteristics are observed. The length and time scales related to the cloud driven mixing are investigated, which are shown to provide additional information about the structure and the source of the mixing inside the boundary layer. They are also shown to place constraints on the length of the sampling periods used to derive products, such as the turbulent dissipation rate, from lidar measurements. For this, the upper cut-off wavelength of the inertial subrange is studied through spectral analysis of the vertical velocity. The bulk statistical profiles and the scaling of the inertial subrange show consistent behaviour as the boundary layer undergoes transitions between a coupled and decoupled stratocumulus layer. The cut-off wavelength of the inertial subrange does not appear to scale robustly with the relative depth of the local mixing regime at different altitudes during decoupled periods. Rather, the competition between surface-based and cloud-driven mixed layers suppresses the range of eddy sizes at all heights inside the boundary layer.

## 1 Introduction

Properties of the turbulent variations in vertical velocity, as well as the scaling related to that variability, are important aspects for understanding boundary layer evolution, transport of momentum and thermodynamical properties. These aspects are tightly coupled to the formation and evolution of boundary layer clouds, which in turn strongly affect the radiation budget of the Earth's surface and thus the climate.

## Turbulence structure in a cloud-topped boundary layer

J. Tonttila et al.

Title Page

Abstract

Introduction

Conclusions

References

Tables

Figures



Back

Close

Full Screen / Esc

Printer-friendly Version

Interactive Discussion



**Turbulence structure  
in a cloud-topped  
boundary layer**

J. Tonttila et al.

[Title Page](#)[Abstract](#)[Introduction](#)[Conclusions](#)[References](#)[Tables](#)[Figures](#)[Back](#)[Close](#)[Full Screen / Esc](#)[Printer-friendly Version](#)[Interactive Discussion](#)

Measurements of the turbulent fluctuations of vertical wind in cloud-topped and clear-sky boundary layers as well as inside boundary layer clouds have been performed for decades, typically making use of in-situ measurement devices mounted on research aircraft (e.g. Duynkerke et al., 1995; Nicholls, 1984, 1989). Unlike in-situ sensors, active remote-sensing instrumentation based at the surface has the significant advantage of being able to routinely measure the velocity profile simultaneously at many levels. A variety of instruments have been employed for this task, from UHF wind-profilers (e.g. Gossard et al., 1998; Jacoby-Koaly et al., 2002) to SODARs (e.g. Kouznetsov et al., 2007), Doppler cloud radars (e.g. Shupe et al., 2012), and combinations of these (e.g. Norton, 2006).

Doppler lidars have the necessary high spatial and temporal resolution to derive turbulent properties (Gal-chen et al., 1992; Banakh et al., 1999); recent developments in this field have resulted in robust low-powered instruments designed to operate continuously and autonomously. They are ideal for boundary layer applications, where they have sufficient sensitivity. Since stratocumulus-topped boundary layers cover a significant portion of the globe, there have been numerous remote-sensing investigations of them in both marine and continental environments (e.g. Babb and Verlinde, 1999; Duynkerke et al., 1995; Frisch et al., 1995; Hogan et al., 2009; Kollias and Albrecht, 2000; Lothon et al., 2006; Moyer and Young, 1991).

In this article we investigate the scaling of turbulent eddies in a stratocumulus-topped boundary layer and its transition between different mixed layer structures. The analysed observations cover a boundary layer exhibiting marine characteristics, with both solid and broken cloud structure in the overlying stratocumulus deck. Doppler lidar measurements are used to analyse the vertical velocity field in the boundary layer below the cloud. The aerosol particles in the marine environment provide an ideal tracer for the Doppler lidar and are present in sufficient quantities to provide measurements at high spatial and temporal resolution with good sensitivity throughout the entire vertical extent from near the surface up to cloud base. This allows for a Fourier analysis of vertical velocity as a function of height. The resulting power spectra are used to in-

**Turbulence structure  
in a cloud-topped  
boundary layer**

J. Tonttila et al.

Title Page

Abstract

Introduction

Conclusions

References

Tables

Figures



Back

Close

Full Screen / Esc

Printer-friendly Version

Interactive Discussion



investigate the relative scaling of the turbulent eddies and contrast them with the bulk statistical properties of the vertical velocity distribution. We can then attempt to link the turbulent variability with the nature of the boundary layer and the overlying cloud deck. Inspired through recent studies by Hogan et al. (2009) and Harvey et al. (2013), who provided observational evidence of how to identify and isolate the cloud driven mixing from surface-based mixing in a stratocumulus topped boundary layer based on the skewness of vertical velocity, we hypothesize that the scaling of the inertial subrange determined from the spectral analysis can be used as an additional diagnostic to identify the sources of turbulent mixing. We also investigate how changes in the structure of the cloud deck affect this scaling in the sub-cloud layer in the situation where the turbulence is cloud-driven.

The layout of this paper is as follows: Sect. 2 describes the instrumentation and the main analysis methods. A description of the synoptic situation and key features during the analysed period is given in Sect. 3. The results obtained for turbulence statistics and the scaling of the inertial subrange are given in Sect. 4, followed by concluding remarks.

## 2 Methodology

### 2.1 Instrument

The data for this study were obtained from a coherent heterodyne pulsed Doppler lidar (production no 34) owned by the Finnish Meteorological Institute, and deployed at Mace Head, on the west coast of Ireland (53°19' N, 9°53' W), from 16 February to 27 March 2012 (Hirsikko et al., 2014). Operating specifications for the Doppler lidar are given in Table 1. Initial data points are oversampled at 3 m resolution and 10 points are then combined to give a final spatial resolution of 30 m. A total of 320 gates gives a maximum range of 9.6 km. The temporal resolution can be as high as 1 s. However, to obtain good sensitivity, it is usually necessary to integrate further, since useful signals

are only obtained in the presence of reasonable aerosol load, or when clouds are present.

The instrument was operated predominantly in the zenith-pointing stare mode, interspersed with a wind scan sequence every 10 min (giving 6 wind profiles per hour).

For this campaign, an integration time of 10 s was selected for the vertical stare mode, sufficiently long for acquiring profiles with reasonably small uncertainties, while short enough for deriving turbulent properties.

As standard, the Doppler lidar provides profiles of signal-to-noise ratio (SNR), uncalibrated attenuated backscatter coefficient and radial Doppler velocity. Post-processing (Hirsikko et al., 2014) then applies background and focus corrections to the signal and provides calibrated attenuated backscatter coefficient profiles, together with uncertainties in the signal, attenuated backscatter and Doppler velocity derived using an approximation to the Cramer-Lao lower-bound method (Rye and Hardesty, 1993) given in O'Connor et al. (2010).

The horizontal wind profiles were obtained using a 3-beam Doppler Beam Swinging (DBS) technique. The wind scan sequence consisted of three consecutive rays, one pointing to the zenith, and two orthogonal rays at 20° from the zenith (one pointing North, one pointing East). Vertical profiles of horizontal winds can then be obtained through trigonometry from radial velocities under appropriate conditions (e.g. Koscielny et al., 1984). As noted in Table 1, to reduce uncertainties in the retrieved horizontal winds, the integration time for each ray in the wind scan sequence was twice the integration time for an individual ray in the zenith-pointing mode. A single vertical profile of horizontal winds therefore took about 60 s to obtain.

Data quality is provided directly by examining SNR (after applying any background correction). The threshold is determined based on the acceptable uncertainty for a given application. For vertically-pointing data, the selected threshold of -21 dB for SNR is equivalent to an uncertainty of about 0.05 m s<sup>-1</sup> for this particular Doppler lidar instrument in this configuration. The Doppler lidar attenuated backscatter coefficient can additionally be calibrated according to a procedure introduced by O'Connor et al.

**Turbulence structure  
in a cloud-topped  
boundary layer**

J. Tonttila et al.

Title Page

Abstract

Introduction

Conclusions

References

Tables

Figures



Back

Close

Full Screen / Esc

Printer-friendly Version

Interactive Discussion



(2004). In this method, the integration of attenuated backscatter from a nearly non-drizzling cloud base through to infinity is set equal to  $1/(2\eta S)$ , where  $\eta$  is the multiple scattering factor and  $S$  is the lidar ratio. Both  $\eta$  (close to 1) and  $S$  (20 sr) are assumed constant and known for this instrument and lidar wavelength in stratocumulus clouds (Westbrook et al., 2010). Drizzling clouds are screened from the calibration procedure by a non-drizzling condition. There it is required that attenuated backscatter coefficient values at 250 m below the cloud base are 10 times smaller than the attenuated backscatter coefficient inside the liquid cloud (O'Connor et al., 2004). The uncertainty in the calibration method is 20 %.

## 2.2 Vertical velocity analysis

The Doppler lidar produces vertical velocity profiles at 10 s resolution. Turbulent properties were derived from statistical properties of the vertical velocity distribution over longer intervals. The properties are computed at every range gate of the lidar giving a high-resolution vertical profile of each turbulent property.

The second and third moments of the velocity distribution, standard deviation  $\sigma_w$  and skewness  $\gamma_w$ , are calculated from sequential vertical velocity samples over a 30 min interval;

$$\sigma_w = \sqrt{\frac{1}{n} \sum_{i=1}^N (w_i - \bar{w})^2}, \text{ and} \quad (1)$$

$$\gamma_w = \frac{\frac{1}{n} \sum_{i=1}^N (w_i - \bar{w})^3}{\sigma_w^3}, \quad (2)$$

respectively, where  $\bar{w}$  is the sample mean vertical velocity and  $w_i$  is the  $i$ th vertical velocity sample. Due to the interspersed sampling of the horizontal wind every 10 min,  $n$  for the 30 min period is in practice about 150.

## Turbulence structure in a cloud-topped boundary layer

J. Tonttila et al.

Title Page

Abstract

Introduction

Conclusions

References

Tables

Figures

◀

▶

◀

▶

Back

Close

Full Screen / Esc

Printer-friendly Version

Interactive Discussion



The vertical velocity power spectrum is used to identify the range of scales over which turbulent mixing predominates, commonly known as the inertial subrange. This is accomplished by finding the cut-off wavelength  $\lambda_0$  at which the spectral slope deviates from the expected  $-5/3$ -powerlaw, as shown schematically in Fig. 1. The spectral model by Kristensen et al. (1989), also applied by Lothon et al. (2009), is used to identify the cut-off wavelength. The model-based spectral intensity as a function of the wavenumber  $k$  is given by

$$S(k) = \frac{\sigma_w^2 l}{2\pi} \frac{\left(3 + 8 \left(\frac{lk}{a}\right)^{2\mu}\right)}{3 \left(1 + \left(\frac{lk}{a}\right)^{2\mu}\right)^{\frac{5}{6\mu} + 1}}, \quad (3)$$

where  $\mu$  controls the curvature of the spectrum. Further,  $a$  is given as a function of  $\mu$ :

$$a(\mu) = \frac{\pi\mu\Gamma\left(\frac{5}{6\mu}\right)}{\Gamma\left(\frac{1}{2\mu}\right)\Gamma\left(\frac{1}{3\mu}\right)}, \quad (4)$$

where  $\Gamma$  is the gamma function. The parameter  $l$  is the integral scale of vertical velocity along the horizontal flow trajectory. In this model,  $l$  can be expressed as a function of  $\lambda_0$  and  $\mu$  (i.e. inverse solution of Eq. (3) in Lothon et al., 2009). The cut-off wavelength can then be normalized by boundary layer height  $z_j$  to give

$$L_0 = \frac{\lambda_0}{z_j}. \quad (5)$$

We create the power spectrum from consecutive velocity samples over the same 30 min interval as for  $\sigma_w$ ,  $\gamma_w$ , and  $z_j$  is taken as the cloud top altitude determined from a coincident Doppler cloud radar (the 35.5 GHz MIRA).

**Turbulence structure  
in a cloud-topped  
boundary layer**

J. Tonttila et al.

Title Page

Abstract

Introduction

Conclusions

References

Tables

Figures



Back

Close

Full Screen / Esc

Printer-friendly Version

Interactive Discussion



We also utilise the turbulent dissipation rate, which is derived from the high temporal resolution vertical velocities (O'Connor et al., 2010):

$$\epsilon = 2\pi \left( \frac{2}{3a_k} \right)^{\frac{3}{2}} \sigma_{\bar{v}}^3 \left( L^{2/3} - L_1^{2/3} \right)^{-3/2}, \quad (6)$$

where  $a_k = 0.55$  is the Kolmogorov constant for one-dimensional wind spectra,  $\sigma_{\bar{v}}$  is the standard deviation of the mean velocity over  $N$  sequential velocity samples,  $L$  is the spatial length scale corresponding to the number of samples used for calculating  $\sigma_{\bar{v}}$ , and  $L_1$  is the length scale appropriate for an individual sample. In this study we use  $N = 12$  samples, which corresponds to an averaging interval of 2 min. The length scales are then computed as  $L = NUt$ , where  $U$  is the horizontal wind speed as measured by the Doppler lidar DBS scan sequence, and  $t$  is the integration time for one ray. Note that  $\sigma_{\bar{v}}$  is calculated over a much shorter time interval than  $\sigma_w$  (2 min vs. 30 min).

### 3 Meteorological conditions and general features

The stratocumulus-topped marine boundary-layer studied here was observed over Mace Head, Ireland, during 24–25 February 2012. The synoptic situation during this period is displayed in Fig. 2. There was a large area of high pressure to the south of Ireland extending west from France out into the Atlantic. To the north were adjacent centres of low pressure west of Iceland and over Scandinavia. The predominant flow over Ireland was from a westerly direction. Our analysis concentrates on the stratocumulus (Sc) clouds emerging after the over-pass of a weak remnant of the tail-end of a precipitating cold front, extending from an occlusion associated with the low pressure centre that had moved from the Northern Atlantic to Eastern Europe by 18:00 UTC on the 24 February (Fig. 2). The passage of the front over Mace Head occurs during the early hours of 24 February, and, by 08:00 UTC, the rain at the surface associated with the front dies out. The remaining mid- and high-level clouds associated with the

## Turbulence structure in a cloud-topped boundary layer

J. Tonttila et al.

Title Page

Abstract

Introduction

Conclusions

References

Tables

Figures



Back

Close

Full Screen / Esc

Printer-friendly Version

Interactive Discussion



**Turbulence structure  
in a cloud-topped  
boundary layer**

J. Tonttila et al.

Title Page

Abstract

Introduction

Conclusions

References

Tables

Figures



Back

Close

Full Screen / Esc

Printer-friendly Version

Interactive Discussion



frontal area have diminished by around 11:00 UTC, as shown by vertically-pointing cloud radar observations in Fig. 3. The passage of the front is also evident in the horizontal wind field observed by the Doppler lidar (Fig. 4) as wind speeds decrease from 15 to  $8 \text{ m s}^{-1}$ . This period between approximately 08:00 UTC to 11:00 UTC appears virtually non-turbulent in the observations of the lower atmosphere; the surface front has already passed, but the boundary-layer is still influenced by the presence of the frontal zone at upper levels. The clouds associated with the frontal zone at upper levels are still present. Due to a moderate horizontal flow from the north-west (approximately  $8 \text{ m s}^{-1}$ ; Fig. 4), a rather shallow surface based mixed layer with marine characteristics is expected over the observation site. The turbulence characteristics observed with the lidar are shown in Fig. 5, in which the profiles of  $\sigma_w$  and  $\epsilon$  indeed indicate the existence of a very shallow mixed layer close to the surface. Above 150 m, the turbulence is very weak with  $\sigma_w \leq 0.1 \text{ m s}^{-1}$  and very low  $\epsilon$ . At these heights, the properties of the flow are more reminiscent of the free tropospheric conditions rather than the boundary layer, although the layer still contains enough particles for a relatively strong lidar signal up to about 1000 m height.

Later during the afternoon of the 24, the north-westerly horizontal flow weakens gradually to about  $4 \text{ m s}^{-1}$  and remains low until 27:00 UTC (counting from 00:00 UTC of the 24 February), when the wind speed starts to increase. The base of the Sc layer is at approximately the height of 1000 m on the 24, as observed by both the lidar and radar (Figs. 5a and 3). During the 22:00–32:00 UTC period, the cloud base height decreases gradually from 1000 m to about 800 m. The 27:00–32:00 UTC period however features a rather uniform cloud structure with almost constant cloud base height. As shown later, this provides an interesting counterpart for the broken cloud structure seen in the afternoon of the 24.

Cloud topped boundary layers can exhibit many different structural types (Lock et al., 2000; Harvey et al., 2013). The boundary layer mixing is defined as coupled when the cloud layer is directly associated with the turbulent mixing originating from the surface due to buoyant or mechanical turbulence generation, or when turbulent mixing driven

**Turbulence structure  
in a cloud-topped  
boundary layer**

J. Tonttila et al.

[Title Page](#)[Abstract](#)[Introduction](#)[Conclusions](#)[References](#)[Tables](#)[Figures](#)[Back](#)[Close](#)[Full Screen / Esc](#)[Printer-friendly Version](#)[Interactive Discussion](#)

by cloud top radiative cooling extends to the below-cloud mixed layer and even all the way down to the surface (Garrat, 1992). The mixing in the boundary layer is defined as decoupled when the cloud driven mixing is not associated with the surface or surface processes. Typically, mixing in and below Sc layers is driven by the longwave radiative cooling of the Sc deck itself, and is important in maintaining the Sc cloud layer through the vertical transport of moisture, especially when there is no substantially strong turbulent vertical transport driven by surface processes.

A broken cloud-deck is evident during the afternoon of the 24 February, caused by breaks between the cellular structure in the stratocumulus advected over the site. The cloud base height shows some variation over time, although mainly less than 150 m, with less variation in cloud top height. We will show later in Sect. 4 that the daytime broken clouds on the 24 are associated with decoupled mixing, while the cloud deck in the morning of the 25 can be regarded as coupled, yet still cloud-driven.

A longer break in the low-level clouds occurs from 18:00–20:00 UTC, which coincides with cirrus clouds emerging over the site. The stratocumulus deck re-emerges when the upper-level cirrus begins to diminish. Unlike the broken field in the cloud deck earlier in the afternoon, which is probably due to internal Sc dynamics, this longer gap appears to be the result of the radiative impact of the cirrus layer above. Christensen et al. (2013) showed that, during night time, on short timescales on the order of a few hours, an upper level cloud significantly decreases the cloud top radiative cooling and the liquid water path of the stratocumulus layer. In essence, part of the up-welling longwave radiation is absorbed and re-emitted downwards by the cirrus and reduces the Sc cloud-top radiative cooling. Without vertical transport of moisture through Sc cloud-top radiative cooling, the Sc layer cannot maintain itself and dissipates. This corresponds very well to our observations, as when the cirrus cloud layer emerging over the Sc deck becomes optically thick, it eventually causes the transitory dissipation of the low-level stratocumulus. Once the cirrus layer is no longer optically thick enough, it does not take long for the Sc layer to return.

## 4 Turbulence structure in coupled and decoupled cloud driven mixed layers

### 4.1 Vertical velocity statistics

The time-height cross-sections of turbulence statistics and lidar attenuated backscatter for the full observation period are shown in Fig. 5. Judging by  $\sigma_w$  and the lidar attenuated backscatter profile, the strongest turbulent variability is generally connected with stratocumulus-topped profiles. It is also evident that  $\sigma_w$  tends to increase towards the cloud deck throughout the observed period. While relatively intense mixing is observed during the 23:00–32:00 UTC period for the whole depth of the boundary layer (with maximum  $\sigma_w = 0.8 \text{ m s}^{-1}$  near the cloud layer and  $0.5 \text{ m s}^{-1}$  also near the surface), the 11:00–18:00 UTC period shows generally weaker mixing and a more pronounced difference between the near-surface and below-cloud layers. The results imply that the mixing is primarily driven by cloud-top radiative cooling (Lock, 1998; Hogan et al., 2009; Harvey et al., 2013), which is commonly observed in midlatitude marine stratocumulus. The profile of  $\epsilon$  and  $\gamma_w$  shown in Fig. 5 support this conclusion. Other processes that have an impact on the cloud-driven mixing include entrainment, although it is often difficult to separate these processes in remote sensing measurements (Kollias and Albrecht, 2000).

Our interpretation of the boundary-layer structure is further supported when examining the skewness profiles in Fig. 5d; negative skewness of vertical velocity, which has been shown to indicate cloud-driven mixing (Hogan et al., 2009), is a predominant feature of the below-cloud mixed layer. Moreover, Hogan et al. (2009) noted that cloud-driven mixing in many ways resembles “upside-down” convective mixing, which is supported by the profiles of  $\sigma_w$  and  $\epsilon$  in Fig. 5. Similar behaviour has also been observed in-cloud, i.e. the peak  $\sigma_w$  is found near the cloud top with negative  $\gamma_w$  (Frisch et al., 1995; Kollias and Albrecht, 2000).

The evolution of the negative  $\gamma_w$  region indicates a difference in the depth of the cloud-driven layer between the afternoon of the 24 February and the night/early morning of the 25 February. A region of positive  $\gamma_w$  extends upwards from the surface during

## Turbulence structure in a cloud-topped boundary layer

J. Tonttila et al.

Title Page

Abstract

Introduction

Conclusions

References

Tables

Figures



Back

Close

Full Screen / Esc

Printer-friendly Version

Interactive Discussion



**Turbulence structure  
in a cloud-topped  
boundary layer**

J. Tonttila et al.

Title Page

Abstract

Introduction

Conclusions

References

Tables

Figures



Back

Close

Full Screen / Esc

Printer-friendly Version

Interactive Discussion



the afternoon of the 24, suggesting the growth of a surface-based mixed layer, although  $\sigma_w$  is rather weak for this region. The growth of the surface-based layer reduces the depth of the cloud-driven portion of the boundary layer with negative  $\gamma_w$ . No such layer of positive skewness is visible during the 25. This indicates that in the afternoon of the 24, the cloud layer becomes decoupled from the surface, while during the night of the 25, the cloud-driven mixing is strong enough to support a coupled layer.

A very shallow surface-driven mixed-layer is expected over the North Atlantic Ocean because the sea surface temperature is cool, especially in February ( $10^\circ\text{C}$ ). With small surface heat fluxes the ocean surface-driven mixed-layer may only reach a couple of hundred meters or so, with minimal diurnal variation. The presence of a cloud-driven mixed-layer would dominate the boundary-layer throughout the diurnal cycle. The surface-driven layer could therefore be below the minimum range of the instrument and not detected (roughly below 100 m). This is in contrast to land-based surface-driven mixed-layers, which exhibit a strong diurnal cycle and can be much deeper due to much larger surface heat fluxes, even if the surface temperature is not much warmer than that over the ocean. A cloud-driven mixed-layer might be expected to dominate the boundary layer over land during night, but the surface-driven layer could be much stronger during the day. The competition between the two mixed-layers can be observed by examining the turbulent parameters,  $\sigma_w$ ,  $\gamma_w$ , and  $\epsilon$  together.

A coastal site with an onshore wind should experience a boundary-layer characteristic of marine environments. This shallow surface-driven mixed-layer is then advected over the coastal site. What then causes the surface-based layer to expand during the 12:00–18:00 UTC period? At least two potential factors are identified. The broken cloud structure seen in the early afternoon could allow increased direct solar surface heating of the coastal observation site, thus promoting growth of the surface mixed-layer. But, due to the close proximity to the ocean and the low angle of the wintertime sun, this effect is most likely weak. The broken cloud structure, and direct solar radiation modifying the temperature profile, could also decrease the production of the turbulent kinetic energy at the top of the cloud layer. However,  $\epsilon$  remains quite high within the

**Turbulence structure  
in a cloud-topped  
boundary layer**

J. Tonttila et al.

Title Page

Abstract

Introduction

Conclusions

References

Tables

Figures



Back

Close

Full Screen / Esc

Printer-friendly Version

Interactive Discussion



upper portion of the cloud-driven mixed-layer throughout this period. In addition, the surface-based layer starts to extend by noon, before there are any obvious gaps in the cloud layer. The key feature to note is that the horizontal wind speed starts to decrease around noon and continues to do so during the afternoon (Fig. 4). With the onshore wind weakening, there is more competition between the shallow marine surface-driven layer and the deeper surface-driven mixed-layer generated inland; the surface-driven mixed-layer above this coastal location is influenced by both weak heat fluxes from the ocean surface and relatively strong heat fluxes from the land, at least during the day. After 18:00 UTC, with no incoming solar radiation, the surface heat fluxes inland are too small to support any surface-driven convection and  $\epsilon$  at the surface is reduced significantly. There is no competition for the cloud-driven mixed-layer, which can now slowly grow again after the cirrus layer departs, and eventually reach the surface.

## 4.2 Scaling of the inertial subrange

We now investigate the scaling of the inertial subrange in the stratocumulus-topped periods and relate those results to the differences in the turbulence statistics described in the previous section. As noted earlier, the boundary layer height  $z_i$  is defined as encompassing the entire boundary layer from the surface to the cloud top altitude, and may contain one or more distinct layers. The cut-off wavelength  $L_0$  is analysed at 30 min intervals at three normalized height levels in the boundary layer, which are at  $0.2 z_i$ ,  $0.5 z_i$  and  $0.8 z_i$ . The scaling of  $L_0$  is presented in Fig. 6 together with the height of the interface between surface and cloud-driven regimes, diagnosed from the height of zero vertical velocity skewness. In addition, Fig. 6 shows the below-cloud mean horizontal wind speed, and black shading indicates the presence of cloud (cloud base is retrieved from the lidar, and cloud top from the cloud radar).

It is not always possible to derive  $L_0$ ; the vertical velocity power-spectra can be very noisy in regions with low lidar signal strength, or  $L_0$  may be below the wavelengths resolved by the spectral decomposition. Moreover, the spectrum may sometimes feature a double peaked structure, in which case the higher wavenumber peak is consid-

**Turbulence structure  
in a cloud-topped  
boundary layer**

J. Tonttila et al.

Title Page

Abstract

Introduction

Conclusions

References

Tables

Figures



Back

Close

Full Screen / Esc

Printer-friendly Version

Interactive Discussion



ered. The presentation of the results is divided into two equal length periods ranging from 08:00 to 20:00 UTC and from 20:00 to 32:00 UTC counting from 00:00 UTC of the 24 February. In an idealized well-mixed boundary layer with isotropic turbulence one might expect to see  $L_0 \approx 1.0$ , which is thus highlighted with a solid blue line in Fig. 6. This expectation arises from the first-order hypothesis that the maximum length scale of the turbulent eddies is of the same order of magnitude as the thickness of the boundary layer (Stull, 1988). As shown below,  $L_0 < 1.0$  tends to indicate a suppression of the development of the turbulent mixed-layer structure. In contrast,  $L_0 > 1.0$  can be interpreted as the impact of larger-scale forcings, e.g. gravity-wave activity, or perhaps stretching of the turbulent eddy structure during changes in wind conditions. As seen in Fig. 6, overall,  $L_0$  varies significantly with time and with height. Yet, a distinct behaviour is observed with respect to the boundary layer structure and the properties of the overlying cloud-deck.

During 08:00–11:00 UTC, just after the passage of the front and before the stratocumulus emerges over the site, there are clear differences with respect to height, with  $L_0 < 0.5$  at  $0.2 z_j$  and  $L_0 \geq 1$  above. This supports the analysis performed in Sect. 3, as it suggests a shallow surface boundary layer with a weakly turbulent, free-tropospheric air mass above, still under synoptic influence of frontal dynamics.

As the stratocumulus layer advects over the area around noon,  $L_0$  is around 1.0–1.4 at all levels for a brief period before a sharp decrease to  $L_0 \approx 0.5$  at 13:00 UTC. This coincides with the appearance of a more broken cloud structure, and the growth of the surface-based layer. It is evident from Fig. 6, that, until 20:00 UTC,  $L_0$  correlates negatively with the height of the zero skewness interface. Periods with a pronounced separation between the surface-based and cloud driven layers, (e.g. 13:00–16:00 UTC) show characteristically smaller  $L_0$ . Furthermore,  $L_0$  values sampled at different levels undergo very similar transitions and have similar magnitudes. The competition between the surface and cloud-driven layers effectively prevents the formation of a well developed mixed layer, and the clear separation between the two regimes constrains the scaling of  $L_0$  to rather low values. No clear differences can be identified in  $L_0$  spe-

cific to the mixing regime sampled, but rather, a decoupled Sc-topped boundary layer structure yields similar suppression of  $L_0$  at all sampled levels.

The situation from 20:00 UTC onwards exhibits somewhat different behaviour. From 20:00–32:00 UTC the cloud-deck is almost continuous and there is no solar influence.

5 The cloud-driven mixed-layer grows downwards to reach the surface by 22:00 UTC and remains within proximity of the surface until around 32:00 UTC (8 a.m. LT). During the initial growth of this cloud-driven mixed-layer  $L_0$  values are generally low, although gradually increasing, and it is not until 28:00 UTC that  $L_0 \approx 1.0$  at all levels.

10 Compared to the daytime period, 12:00–16:00 UTC, at night there is no competition for the cloud-driven layer as it develops. Rather, the mixed layer can expand downwards quite freely, which is why the suppression of  $L_0$  from 20:00–26:00 UTC is surprising. This may be due to the low horizontal wind speeds, about  $4 \text{ m s}^{-1}$ , which may be affecting entrainment processes and thus the dimensions of the cloud-driven turbulence. The gradual increase in  $L_0$  during 24:00–32:00 UTC coincides with the increase in horizontal wind speed. The intensifying wind changes the aspect ratio of the turbulent eddies by stretching the updraft and downdrafts further apart horizontally. Additionally, winds modulate the entrainment process, with intense entrainment causing strong evaporative cooling. This then modifies the production of turbulent energy at the top of the boundary layer (Lock, 1998), which can also affect the scaling of  $L_0$  in the cloud-driven environment.

20 Local sunrise is about 7.40 a.m. (31:40 UTC in Fig. 6). A new surface-driven mixed layer starts to grow, evident through positive skewness and a change in dissipation rate in Fig. 5. Although the dissipation rate suggests that this surface-driven layer is less turbulent than the cloud-driven mixed-layer, it continues to grow into, and erode the cloud-driven layer. Note that  $L_0$  at all levels is abruptly reduced to 0.5. Towards the noon of the 25 the situation is under increasing influence of a gradual air mass change, explaining the reduction in cloud-base height. Related to this, Fig. 3 shows evidence of an enhanced drizzle production, which strongly affects the mixed-layer dynamics, making this situation very different from the earlier analysed periods.

**Turbulence structure  
in a cloud-topped  
boundary layer**

J. Tonttila et al.

Title Page

Abstract

Introduction

Conclusions

References

Tables

Figures



Back

Close

Full Screen / Esc

Printer-friendly Version

Interactive Discussion



**Turbulence structure  
in a cloud-topped  
boundary layer**

J. Tonttila et al.

Title Page

Abstract

Introduction

Conclusions

References

Tables

Figures



Back

Close

Full Screen / Esc

Printer-friendly Version

Interactive Discussion



The consequences of the variation in  $L_0$  can be outlined by examining the advective time-scales corresponding to the cut-off wavelength of the inertial subrange,  $\lambda_0$ . The time-scales are shown in Fig. 7, and are obtained by dividing  $\lambda_0$  by the collocated wind speed (averaged over 1 h and 100 m in the vertical). The majority of the timescales reside between 100 and 300 s. As may be expected, time-scales at the lowest height sampled here,  $0.2 z_j$ , are usually smaller than those above, but this is not always the case, especially in decoupled situations when there are two or more discrete mixed-layers. Knowledge of this time-scale is important when calculating derived products, such as the dissipation rate, from the measurements, where it is assumed that all sampled length scales are within the inertial subrange. More samples would be preferred for more robust statistics, but as indicated in Fig. 7, complex boundary layer structures exhibit a wide variation in the length scales which reside within the inertial subrange, especially in the presence of competing mixed layers. As an example, when deriving dissipation rate using the method of O'Connor et al. (2010), extending the sampling time beyond 3 min would imply that the spatial length scale  $L$  in Eq. (6) is outside the inertial subrange, rendering the assumption used in the derivation of the equation invalid.

## 5 Conclusions

This study analysed two days (24–25 February 2012) of continuous high-resolution Doppler lidar observations from Mace Head, comprising a long-lived stratocumulus cloud deck following behind an overpass of a cold front.

We focused on the turbulent properties exhibited by the cloud-topped boundary layer through examining various parameters derived from the Doppler lidar vertical velocities. Power spectrum analysis of the vertical velocity was also performed to infer the range of scales of mixing associated with the inertial subrange by defining a cut-off wavelength  $L_0$  normalized by the boundary layer depth.

**Turbulence structure  
in a cloud-topped  
boundary layer**

J. Tonttila et al.

Title Page

Abstract

Introduction

Conclusions

References

Tables

Figures



Back

Close

Full Screen / Esc

Printer-friendly Version

Interactive Discussion



From previous studies (Hogan et al., 2009) it is known, that negative skewness of vertical velocity below cloud layer indicates turbulent mixing driven by cloud-top radiative cooling. During the 24 February, a broken cloud structure was observed in the stratocumulus deck, causing weaker production of turbulent kinetic energy at the top of the boundary layer. Together with decreasing horizontal winds on the afternoon of the 24 February, this decreased the depth of the cloud-driven mixed layer, and allowed a weak surface-driven mixed layer to grow (indicated by positive vertical velocity skewness). In effect, the cloud deck was decoupled from the surface. In contrast, at night on the 24–25, the solid stratocumulus deck was essentially coupled to the surface, even though the mixing was cloud-driven, as the mixed-layer grew to encompass the entire depth of the boundary layer.

The investigation of the cut-off wavelength scale  $L_0$  through spectral analysis suggests that a decoupled structure strongly suppresses  $L_0$  at all altitudes. The marked separation between the surface-based and the cloud-driven mixed layers was accompanied by a broken cloud structure and rather weak horizontal winds, with  $L_0$  typically near 0.5 at all heights within the boundary layer. Local intensification of the cloud-driven mixing and the subsequent increase in the depth of the cloud-driven mixed-layer seen during the afternoon of the 24 February were accompanied with sharp increases in  $L_0$ .

In comparison, periods with a well-developed coupled (yet cloud-driven) nocturnal mixed layer showed  $L_0 \approx 1.0$  throughout the boundary layer, even though before the intensification of the horizontal wind,  $L_0$  stayed relatively low. This shift is likely the result of shear stress affecting the geometry of the turbulent eddies with increasing wind and also the production of turbulent kinetic energy at cloud top due to changes in entrainment.

Prior to the campaign, it was expected that  $L_0$  would broadly track the fractional depth of the surface- or cloud-driven layer in which the measurement was made. Although this was observed in some situations, typically decoupled layers with competing mixing regimes (13:00–15:00 and 17:00–22:00 UTC), it was not a robust indicator on its own. However, the results show that vertically resolved  $L_0$  could provide an additional tool to

identify and confirm the structural features of complex cloud-topped boundary layers. In addition, the identification of potential rapid variations in  $L_0$  and the reductions seen in decoupled situations are an important consideration when calculating products such as turbulent dissipation rate because of the resulting constraints on the sampling interval for deriving these parameters.

*Acknowledgements.* This work has been supported by a Väisälä foundation grant from the Finnish Academy of Science and Letters as well as the ERC project PBL-PMES (Grant number 227915). The research leading to these results has also received funding from the European Union Seventh Framework Programme (FP7/2007–2013) under grant agreement no 262254. We thank ACTRIS Transnational Access, the Irish EPA, and the Irish Higher Education Authority for their support, and acknowledge the Met Office Library and Archive for the surface analysis chart.

## References

- Babb, D. M. and Verlinde, J.: Vertical velocity statistics in continental stratocumulus as measured by a 95 GHz radar, *Geophys. Res. Lett.*, 86, 1177–1180, 1999. 24122
- Banakh, V. A., Smalikho, I. N., Köpp, F., and Werner, C.: Measurements of Turbulent Energy Dissipation Rate with a CW Doppler Lidar in the Atmospheric Boundary Layer, *J. Atmos. Ocean. Tech.*, 16, 1044–1061, 1999. 24122
- Christensen, M. W., Carrió, G. G., Stephens, G. L., and Cotton, W. R.: Radiative impacts of free-tropospheric clouds on the properties of marine stratocumulus, *J. Atmos. Sci.*, 70, 3102–3118, doi:10.1175/JAS-D-12-0287.1, 2013. 24129
- Duykerke, P. G., Zhang, H., and Jonker, P. J.: Microphysical and turbulent structure of nocturnal stratocumulus as observed during ASTEX, *J. Atmos. Sci.*, 52, 2763–2777, 1995. 24122
- Frisch, A. S., Lenschow, D. H., Fairall, C. W., Schubert, W. H., and Gibson, J. S.: Doppler radar measurements of turbulence in marine stratiform cloud during ASTEX, *J. Atmos. Sci.*, 52, 2800–2808, 1995. 24122, 24130
- Gal-Chen, T., Xu, M., and Eberhard, W. L.: Estimations of atmospheric boundary layer fluxes and other turbulence parameters from Doppler lidar data, *J. Geophys. Res.*, 97, 18409–18423, 1992. 24122

## Turbulence structure in a cloud-topped boundary layer

J. Tonttila et al.

Title Page

Abstract

Introduction

Conclusions

References

Tables

Figures



Back

Close

Full Screen / Esc

Printer-friendly Version

Interactive Discussion



- Garrat, J. R.: The Atmospheric Boundary Layer, Cambridge University Press, New York, USA, 316 pp., 1992. 24129
- Gossard, E. E., Wolfe, D. E., Moran, K. P., Paulus, R. A., Anderson, K. D., and Rogers, L. T.: Measurement of clear-air gradients and turbulence properties with radar wind profilers, J. Atmos. Ocean. Tech., 15, 321–342, 1998. 24122
- Harvey, N. J., Hogan, R. J., and Dacre, H. F.: A method to diagnose boundary-layer type using Doppler lidar, Q. J. Roy. Meteor. Soc., 139, 1681–1693, doi:10.1002/qj.2068, 2013. 24123, 24128, 24130
- Hirsikko, A., O'Connor, E. J., Komppula, M., Korhonen, K., Pfüller, A., Giannakaki, E., Wood, C. R., Bauer-Pfundstein, M., Poikonen, A., Karppinen, T., Lonka, H., Kurri, M., Heinonen, J., Moisseev, D., Asmi, E., Aaltonen, V., Nordbo, A., Rodriguez, E., Lihavainen, H., Laaksonen, A., Lehtinen, K. E. J., Laurila, T., Petäjä, T., Kulmala, M., and Viisanen, Y.: Observing wind, aerosol particles, cloud and precipitation: Finland's new ground-based remote-sensing network, Atmos. Meas. Tech., 7, 1351–1375, doi:10.5194/amt-7-1351-2014, 2014. 24123, 24124
- Hogan, R. J., Grant, A. L., Illingworth, A. J., Pearson, G. N., and O'Connor, E. J.: Vertical velocity variance and skewness in clear and cloud-topped boundary layers as revealed by Doppler lidar, Q. J. Roy. Meteor. Soc., 135, 635–643, doi:10.1002/qj.413, 2009. 24122, 24123, 24130, 24136
- Jacoby-Koaly, S., Campistron, B., Bernard, S., Benech, B., Ardhuin-Girard, F., Dessens, J., Dupont, E., and Carissimo, B.: Turbulent dissipation rate in the boundary layer via UHF wind profiler Doppler spectral width measurements, Bound.-Lay. Meteorol., 103, 361–389, 2002. 24122
- Kollias, P. and Albrecht, B.: The turbulence structure in continental stratocumulus cloud from millimeter-wavelength radar observations, J. Atmos. Sci., 57, 2417–2433, 2000. 24122, 24130
- Koscielny, A. D., Doviak, R. J., and Zrnić, D. S.: An evaluation of the accuracy of some radar wind profiling techniques, J. Atmos. Ocean. Tech., 1, 309–320, 1984. 24124
- Kouznetsov, R., Kramar, V. F., and Kallistratova, M. A.: The vertical structure of turbulent momentum flux in the lower part of the atmospheric boundary layer, Meteorol. Z., 16, 367–373, 2007. 24122

**Turbulence structure  
in a cloud-topped  
boundary layer**

J. Tonttila et al.

Title Page

Abstract

Introduction

Conclusions

References

Tables

Figures



Back

Close

Full Screen / Esc

Printer-friendly Version

Interactive Discussion



## Turbulence structure in a cloud-topped boundary layer

J. Tonttila et al.

Title Page

Abstract

Introduction

Conclusions

References

Tables

Figures



Back

Close

Full Screen / Esc

Printer-friendly Version

Interactive Discussion



- Kristensen, L., Lenschow, D. H., Kirkegaard, P., and Courtney, M.: The spectral velocity tensor for homogeneous boundary layer turbulence, *Bound.-Lay. Meteorol.*, 47, 149–193, 1989. 24126
- Lock, A. P.: The parameterization of entrainment in cloudy boundary layers, *Q. J. Roy. Meteor. Soc.*, 124, 2729–2753, 1998. 24130, 24134
- Lock, A. P., Brown, A. R., Bush, M. R., Martin, G. M., and Smith, R. N. B.: A new boundary layer mixing scheme. Part I: Scheme description and single-column model tests, *Mon. Weather Rev.*, 128, 3187–3199, 2000. 24128
- Lothon, M., Lenschow, D. H., and Mayor, S. D.: Coherence and scale of vertical velocity in the convective boundary layer from a Doppler lidar, *Bound.-Lay. Meteorol.*, 121, 521–536, doi:10.1007/s10546-006-9077-1, 2006. 24122
- Lothon, M., Lenschow, D. H., and Mayor, S. D.: Doppler lidar measurements of vertical velocity spectra in the convective planetary boundary layer, *Bound.-Lay. Meteorol.*, 132, 205–226, doi:10.1007/s10546-009-9398-y, 2009. 24126
- Moyer, K. A. and Young, G. S.: Observations of vertical velocity skewness within the marine stratocumulus-topped boundary layer, *J. Atmos. Sci.*, 48, 403–410, 1991. 24122
- Nicholls, S.: The dynamics of stratocumulus: aircraft observations and comparisons with a mixed layer model, *Q. J. Roy. Meteor. Soc.*, 110, 783–820, 1984. 24122
- Nicholls, S.: The structure of radiatively driven convection in stratocumulus, *Q. J. Roy. Meteor. Soc.*, 115, 487–511, 1989. 24122
- Norton, E. G., Vaughan, G., Methven, J., Coe, H., Brooks, B., Gallagher, M., and Longley, I.: Boundary layer structure and decoupling from synoptic scale flow during NAMBLEX, *Atmos. Chem. Phys.*, 6, 433–445, doi:10.5194/acp-6-433-2006, 2006. 24122
- O'Connor, E. J., Illingworth, A. J., and Hogan, R. J.: A technique for autocalibration of cloud lidar, *J. Atmos. Ocean. Tech.*, 21, 777–786, 2004. 24124, 24125
- O'Connor, E. J., Illingworth, A. J., Brooks, I. M., Westbrook, C. D., Hogan, R. J., Davies, F., and Brooks, B. J.: A method for estimating the turbulent kinetic energy dissipation rate from a vertically pointing Doppler lidar, and independent evaluation from balloon-borne in situ measurements, *J. Atmos. Ocean. Tech.*, 27, 1652–1664, doi:10.1175/2010JTECHA1455.1, 2010. 24124, 24127, 24135
- Rye, B. J. and Hardesty, R. M.: Discrete spectral peak estimation in incoherent backscatter heterodyne lidar. I: Spectral accumulation and the Cramer-Rao lower bound, *IEEE T. Geosci. Remote*, 31, 16–27, 1993. 24124

Shupe, M. D., Brooks, I. M., and Canut, G.: Evaluation of turbulent dissipation rate retrievals from Doppler Cloud Radar, Atmos. Meas. Tech., 5, 1375–1385, doi:10.5194/amt-5-1375-2012, 2012. 24122

Stull, R. B.: An Introduction to Boundary Layer Meteorology, Kluwer Academic Publishers, Dordrecht, the Netherlands, 666 pp., 1988. 24133

Westbrook, C. D., Illingworth, A. J., O'Connor, E. J., and Hogan, R. J.: Doppler lidar measurements of oriented planar ice crystals falling from supercooled and glaciated cloud layers, Q. J. Roy. Meteor. Soc., 136, 260–276, 2010. 24125

ACPD

14, 24119–24148, 2014

## Turbulence structure in a cloud-topped boundary layer

J. Tonttila et al.

Title Page

Abstract

Introduction

Conclusions

References

Tables

Figures



Back

Close

Full Screen / Esc

Printer-friendly Version

Interactive Discussion





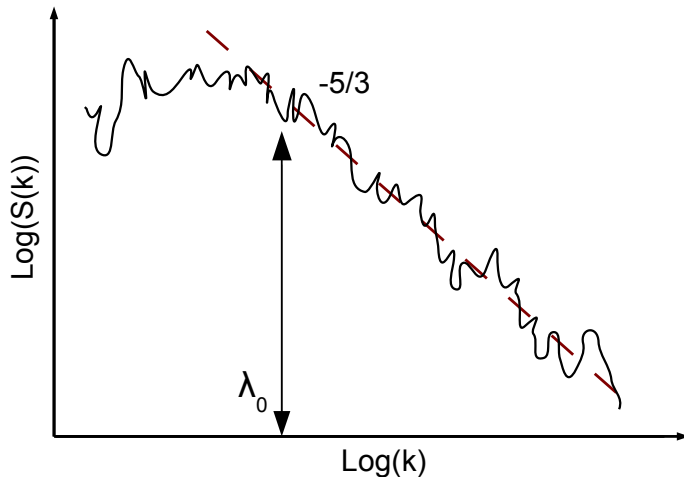


**Figure 1.** A schematic figure of a vertical velocity power spectral density ( $S$ ) as a function of the wavenumber  $k$ . The red dashed line indicates the  $-5/3$  slope, fitted on top of the spectrum on the wavelengths that belong to the inertial subrange. Also depicted is the cut-off wavelength of the inertial subrange ( $\lambda_0$ ).

**Turbulence structure in a cloud-topped boundary layer**

J. Tonttila et al.

Title Page	
Abstract	Introduction
Conclusions	References
Tables	Figures
◀	▶
◀	▶
Back	Close
Full Screen / Esc	
Printer-friendly Version	
Interactive Discussion	



## Turbulence structure in a cloud-topped boundary layer

J. Tonttila et al.

Title Page

Abstract

Introduction

Conclusions

References

Tables

Figures



Back

Close

Full Screen / Esc

Printer-friendly Version

Interactive Discussion

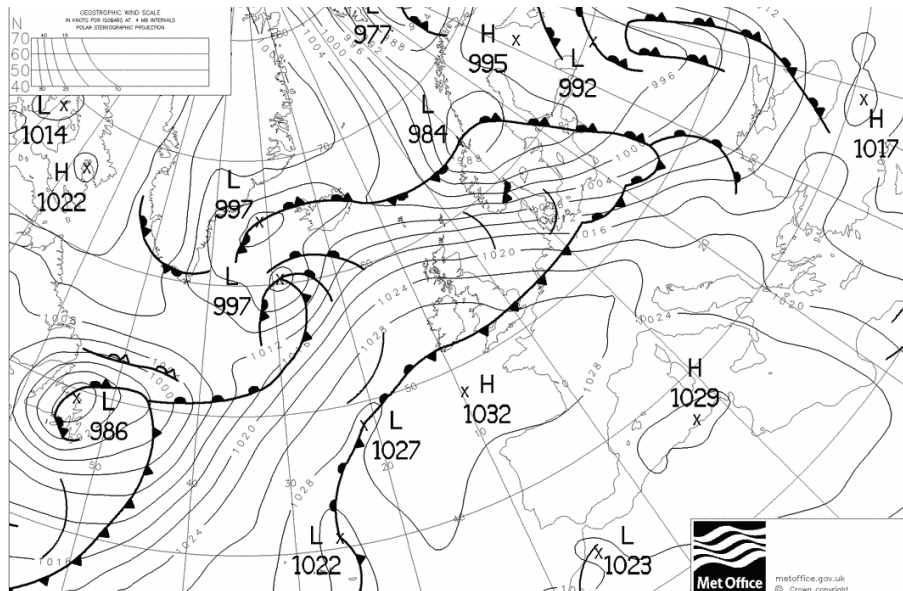


**Figure 2.** Met Office surface analysis chart for 18:00 UTC on 24 February 2012. (© 2012 Crown Copyright, Met Office.)



## Turbulence structure in a cloud-topped boundary layer

J. Tonttila et al.

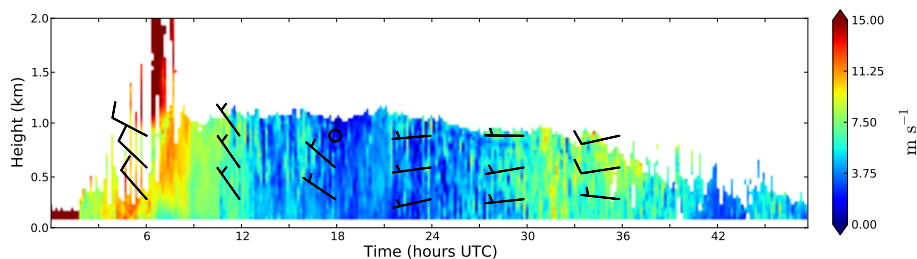


**Figure 4.** Profile of horizontal wind over the analysed two-day period. Wind speed is given by the colormap and wind direction is indicated by the wind barbs.

[Title Page](#)[Abstract](#)[Introduction](#)[Conclusions](#)[References](#)[Tables](#)[Figures](#)[Back](#)[Close](#)[Full Screen / Esc](#)[Printer-friendly Version](#)[Interactive Discussion](#)

## Turbulence structure in a cloud-topped boundary layer

J. Tonttila et al.

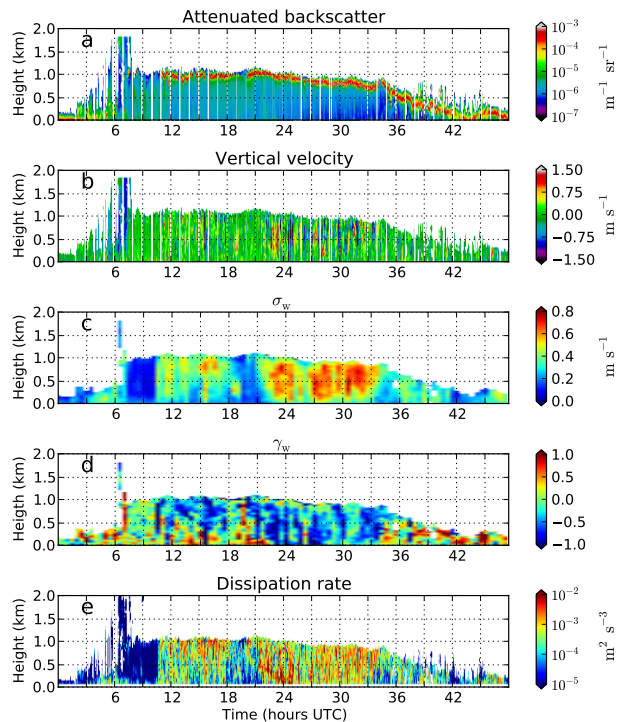


**Figure 5.** (a) Lidar backscatter, (b) Doppler velocity, (c) standard deviation and (d) skewness of vertical velocity and (e) turbulence dissipation rate.

Title Page

Abstract

Introduction

Conclusions

References

Tables

Figures



Back

Close

Full Screen / Esc

Printer-friendly Version

Interactive Discussion



## Turbulence structure in a cloud-topped boundary layer

J. Tonttila et al.

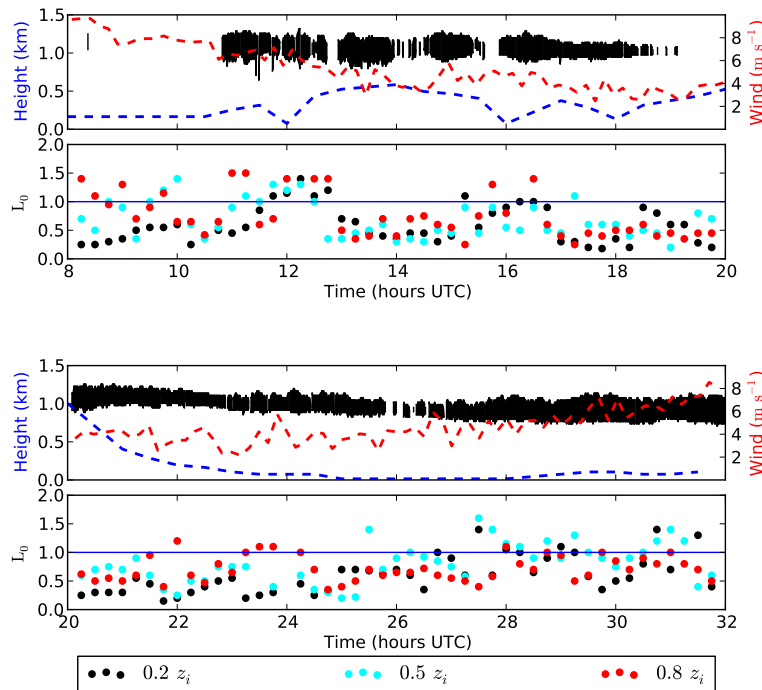


**Figure 6.** Scaling of the inertial subrange with the location and extent of the cloud layer as diagnosed using combined sets of lidar and radar measurements. Clouds are shown in the upper panel as the black shaded area. Blue dashed line represents the interface between surface based and cloud driven mixed layers diagnosed from the profiles of skewness. Red dashed line shows the mean wind speed in the below-cloud layer. The lower panel shows the normalized cut-off wavelength of the inertial subrange ( $L_0$ ) with samples from  $0.2 z_i$  shown in black,  $0.5 z_i$  in light blue and  $0.8 z_i$  in red markers.

**Turbulence structure  
in a cloud-topped  
boundary layer**

J. Tonttila et al.

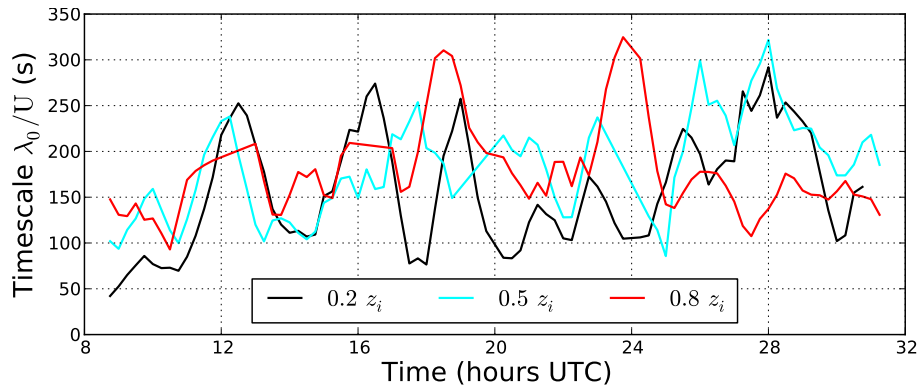


**Figure 7.** Advective time-scales corresponding to the largest scales within the inertial subrange ( $\lambda_0$ ) shown in Fig. 6 from three heights. Time-scales from  $0.2 z_i$  are shown in black,  $0.5 z_i$  in light blue and  $0.8 z_i$  in red.

[Title Page](#)[Abstract](#)[Introduction](#)[Conclusions](#)[References](#)[Tables](#)[Figures](#)[◀](#)[▶](#)[◀](#)[▶](#)[Back](#)[Close](#)[Full Screen / Esc](#)[Printer-friendly Version](#)[Interactive Discussion](#)